

# Multi-Mapping Image-to-Image Translation with Central Biasing Normalization

Xiaoming Yu, Zhenqiang Ying, *Student Member, IEEE*, Ge Li, *Member, IEEE*, and Wen Gao, *Fellow, IEEE*

**Abstract**—Recent image-to-image translation tasks attempt to extend the model from one-to-one mapping to multiple mappings by injecting latent code. Based on the mathematical formulation of networks with existing way of latent code injection, we show the role of latent code is to control the mean of the feature maps after convolution. Then we find common normalization strategies might reduce the diversity of different mappings or the consistency of one specific mapping, which is not suitable for the multi-mapping tasks. We provide the mathematical derivation that the effects of latent code are eliminated after instance normalization and the distributions of the same mapping become inconsistent after batch normalization. To address these problems, we present *consistency within diversity* design criteria for multi-mapping networks and propose *central biasing normalization* by applying a slight yet significant change to existing normalization strategies. Instead of spatial replicating and concatenating into the input layers, we inject the latent code into the normalization layers where the offset of feature maps is eliminated to ensure the output consistency for one specific mapping and the bias calculated by latent code is appended to achieve the output diversity for different mappings. In this way, not only is the proposed design criteria met, but the modified generator network has much smaller number of parameters. We apply this technique to multi-modal and multi-domain translation tasks. Both quantitative and qualitative evaluations show that our method outperforms current state-of-the-art methods. Code and pretrained models are available at <https://github.com/Xiaoming-Yu/cbn>.

**Index Terms**—Normalization, image-to-image translation, multiple mappings.

## I. INTRODUCTION

MANY image processing and computer vision problems can be framed as image-to-image translation tasks [1], mapping an image from one specific domain to another, *e.g.*, facial attributes transform, grayscale image colorization and edge maps to photos. Although recent studies have shown remarkable success in image-to-image translation for two domains [1]–[6], these one-to-one mapping methods are not suitable for multi-mapping problem since different models need to be built for every pair of mapping, even though some mappings share common semantics. To address the problem, latent code is introduced to indicate different mappings and

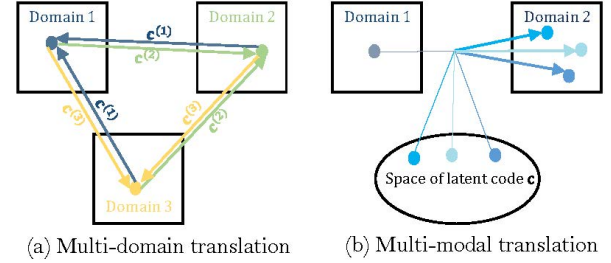


Fig. 1. An illustration of multi-mapping indicated by latent code  $c$ . (a) Multi-domain translation indicated by limited domain latent code. (b) Cross-domain translation indicated by potential attribute latent code.

applied to multi-domain translation tasks [7], [8] and multi-modal translation tasks [9].

Latent code can be a discrete variable that indicates the target domain in the multi-domain translation tasks. Given training data from several different domains, multi-domain models learn to translate images from one domain to the other. As shown in Fig. 1(a), there are three possible latent code corresponding to three target domains. Facial attribute transform is a typical multi-domain task where the domain can represent different hair colors, as shown in Fig. 2(a).

Latent code can also be a continuous variable that indicates the target attribute value in the multi-modal translation tasks. The cross-domain mapping is multimodal in many scenarios such as edge-to-photos, labels-to-photos and night-to-day, as shown in Fig. 2(b). In this case, the latent code is sampled from a continuous attribute space reflecting intra-domain diversity, rather than a discrete domain set reflecting inter-domain diversity, as shown in Fig. 1(b).

Determining how to inject the latent code to the network architecture is a key problem for designing multi-mapping models. Although existing methods present impressive results, we found that they are sensitive to different padding and normalization strategies. In this work, we focus on modeling the effective mapping indicated by latent code. By replacing the common way of Latent Code Injection (LCI) with Central Biasing Normalization, we show it is possible to learn multiple mappings in a network without careful thinking of the structures, such as padding and normalization strategies. Through quantitatively and qualitatively evaluated on two kind of multi-mapping tasks, we demonstrate that our approach is more effective and robust than the common latent code injection methods.

In summary, our paper makes the following contributions:

- We derive the role of latent code in multi-mapping tasks is

This work was supported by the grant of National Science Foundation of China (No.U1611461), Shenzhen Peacock Plan (20130408-183003656), and Science and Technology Planning Project of Guangdong Province, China (No. 2014B090910001). This paper was recommended by Associate Editor X. XX.

X. Yu, Z. Ying, G. Li, and W. Gao are with the School of Electronic and Computer Engineering, Shenzhen Graduate School, Peking University, 518055 Shenzhen, China (e-mail: xiaoming@pku.edu.cn; zqying@pku.edu.cn; geli@ece.pku.edu.cn; wgao@pku.edu.cn).

Color versions of one or more of the figures in this paper are available online at <http://ieeexplore.ieee.org>.

Digital Object Identifier XX.XXXX/XXX.20XX.XXXXXXX

Manuscript received XXX XX, 20XX; revised XXX XX, 20XX.



Fig. 2. Multi-mapping image-to-image translation tasks. (a) The multi-domain translation results of different hair colors (black, blond, brown). (b) The cross-domain translation with multi-modal results. The first two rows present the `edge2photo` translation task, next row is the `label2photo` task and remaining is the `night2day` task. The results in same task are generated by a single generator with central biasing normalization.

to control the mean of the feature maps after convolution.

- As far as we know, we are the first to point out the potential problems of latent code injection.
- Based on two design criteria, we propose central biasing normalization as an alternative way of injecting latent code.

## II. RELATED WORK

In recent years, convolutional neural nets (CNNs) are widely used for various image processing problems. By minimizing the objective that scores the quality of results, CNNs try to model the mapping between the source and target domain. But it is difficult to manually design a effective and universal evaluation objective for different tasks, more and more researchers pay attention to generative adversarial networks (GANs), since GANs optimize the object that adapts to the data.

### A. Generative Adversarial Networks

By staging a zero-sum game, GANs have shown impressive results in image generation [10]–[15]. The extension of GANs with conditional settings have achieved impressive results in various conditional generation tasks such as image inpainting [16], super-resolution [17], text2image [18], and image editing [19].

### B. Image-to-Image Translation

Encouraged by the development of GANs and conditional GANs, previous studies focus on the paired [1] and unpaired image-to-image translation tasks [3]–[6]. Pix2pix [1] uses cGAN [20] to perform supervised learning with data pairs. CycleGAN [3], DiscoGAN [5], and DualGAN [4] enforce cycle consistency for unpaired image-to-image translation. UNIT

[6] combines variational autoencoders [21] with CoGAN [22] to learn a joint distribution of images in different domains. These studies have promoted the development of one-to-one mapping image translation but show limited scalability for multi-mapping translation.

### C. Multiple Mappings

To achieve a more scalable approach for image-to-image translation, significant progress has been made recently in the development of multi-mapping translation [7]–[9]. For instance, StarGAN [8] uses a single model and latent code to achieve multiple domains image-to-image translations. It trains the generator with the discriminator that combines an auxiliary classifier [23], which encourages the learning of multi-mapping indicated by the latent code. Fader Networks [7] use the attribute-invariant representations, encoded by the input image, and the latent code for image reconstruction. BicycleGAN [9] combines VAE-GAN objects [24] and LR-GAN objects [12], [25], [26] for encouraging a bijective mapping between the latent code and output spaces. The common feature of these tasks is to learn a joint distribution between input images and latent code, so it is important to use the latent code by a reasonable way. Existing approaches focus on the training skills but ignore this detail, which may lead to the destruction of their models. We discuss this problem in Sect. IV and compare our method with StarGAN and BicycleGAN in Sect. VI.

## III. REVISIT LATENT CODE INJECTION

For controlling multiple attributes of the generated image, a meaningful vector  $\mathbf{c}$  called latent code is usually used to target the salient structured semantic features. For instance, when generating the facial image, the latent code  $\mathbf{c}$  will indicate

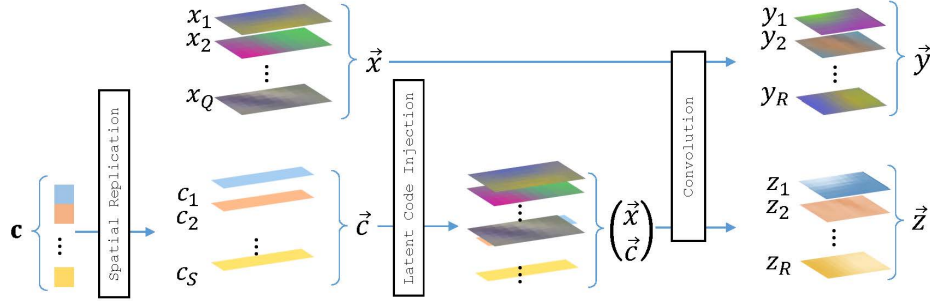


Fig. 3. Convolution operation without/with latent code. The above illustration shows the common convolution without latent code, and the bottom illustrate the convolution operation with latent code injection.

the features we need, like the gender, the hair color or the expression. In existing models for multi-mapping problem, latent code  $c$  is injected by spatial replication and concatenation into the input of convolutional neural network. A typical operation pipeline of the latent code injection network contains Convolution, Normalization and Activation. In common one-to-one mapping translation task, the input volume only contains the source data, but when we use LCI to perform multi-mapping translation, the input volume also contains the target domain information. In this section, we will explain how Latent Code Injection works with convolution and normalization, but ignore the activation since it does not affect our analysis afterwards.

#### A. Convolution Operation without Latent Code

Following the notation of Convolutional Matrix Multiplication (Convolutional MM) [27], we extend the matrix of numbers to the matrix of feature maps or convolution kernels. Here, each element is a feature map or a convolution kernel instead of a number.

Let  $x_1, x_2, \dots, x_Q$  be the  $Q$  input feature maps and  $w_{r,q}$  the  $R \times Q$  convolution kernels (each sized  $K \times L$ ) where  $r = 1, 2, \dots, R$  and  $q = 1, 2, \dots, Q$ , then their convolution operation can be represented as

$$\begin{aligned} y_1 &= w_{1,1} * x_1 + w_{1,2} * x_2 + \dots + w_{1,Q} * x_Q \\ y_2 &= w_{2,1} * x_1 + w_{2,2} * x_2 + \dots + w_{2,Q} * x_Q \\ &\vdots \\ y_R &= w_{R,1} * x_1 + w_{R,2} * x_2 + \dots + w_{R,Q} * x_Q, \end{aligned} \quad (1)$$

where  $y_1, y_2, \dots, y_R$  be the  $R$  output feature maps,  $w_{r,q} * x_q$  is the convolution between a kernel  $w_{r,q}$  and a feature map  $x_q$ . Further, it can be redefined as a special matrix/vector multiplication

$$\vec{y} = W \times \vec{x}, \quad (2)$$

where  $\vec{x} = (x_1, x_2, \dots, x_Q)^T$ ,  $\vec{y} = (y_1, y_2, \dots, y_R)^T$ , and

$$W = \begin{pmatrix} w_{1,1} & w_{1,2} & \dots & w_{1,Q} \\ w_{2,1} & w_{2,2} & \dots & w_{2,Q} \\ \vdots & \vdots & \ddots & \vdots \\ w_{R,1} & w_{R,2} & \dots & w_{R,Q} \end{pmatrix}.$$

#### B. Convolution Operation with Latent Code

For latent code injection networks, the latent code  $c$  of length  $S$  will be replicated and expanded as a special vector  $\vec{c}$  and each feature map of  $\vec{c}$  is a constant channel that every element has same value, as shown in Fig.3. We denote the  $R \times S$  convolution kernels associated with the latent code as  $v_{r,s}$  where  $s = 1, 2, \dots, S$ . Then the convolution multiplication with latent code is

$$\vec{o} = V \times \vec{c}, \quad (3)$$

where  $\vec{c} = (c_1, c_2, \dots, c_S)^T$ ,  $\vec{o} = (o_1, o_2, \dots, o_R)^T$ , and

$$V = \begin{pmatrix} v_{1,1} & v_{1,2} & \dots & v_{1,S} \\ v_{2,1} & v_{2,2} & \dots & v_{2,S} \\ \vdots & \vdots & \ddots & \vdots \\ v_{R,1} & v_{R,2} & \dots & v_{R,S} \end{pmatrix}.$$

Note each feature map  $o_r$  is a constant channel as it is the linear combination of feature maps from  $\vec{c}$ :

$$o_r = v_{r,1} * c_1 + v_{r,2} * c_2 + \dots + v_{r,S} * c_S. \quad (4)$$

The convolution operation from input  $\vec{x}$  and  $\vec{c}$  can be represented as

$$\vec{z} = (W, V) \times \begin{pmatrix} \vec{x} \\ \vec{c} \end{pmatrix} = \vec{y} + \vec{o}, \quad (5)$$

where  $\vec{z} = (z_1, z_2, \dots, z_R)^T$  is the final convolution output.

There are two key observations about the latent code. First, the role of latent code  $c$  is independent of the input  $\vec{x}$  in convolution operation. Second, different latent code only provide different offsets to the output feature maps. In other words, the network needs to distinguish different mappings based on the mean of feature maps.

#### C. Normalization

1) *Batch Normalization*: To accelerate training and improve the performance of deep network, Ioffe and Szegedy introduced the batch normalization (BN) [28] to reduce the internal covariate shift [29] of network by normalizing the feature statistics. Although BN is designed to ease the training of discriminative networks, it also been found effective in deep generative model [15]. In the training stage, the input

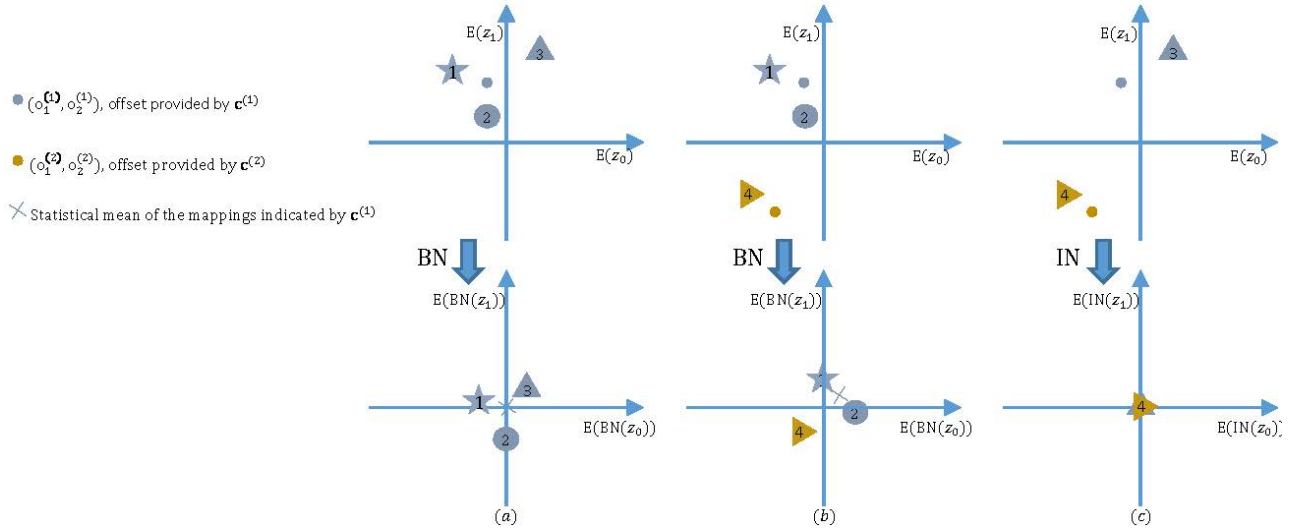


Fig. 4. A toy visualization that only two dimensions are shown for potential problems of LCI model. The first row in these sub-figure is the output of convolution with normalization. The second row is the output with different normal operations. It should be noticed the location of  $z^{(3)}$  is same with  $z^{(4)}$  in the second row of sub-figure(c).

minibatch mean and variance are used to normalize each feature map of the convolutional output:

$$\text{BN}(z_r) = \frac{z_r - \mathbb{E}[Z_r]}{\sqrt{\text{Var}[Z_r]}}, \quad (6)$$

where  $Z_r = (z_r^{(1)}, z_r^{(2)}, \dots)$  is the batch of  $r$ -th feature map. During the inferencing stage, BN replaces the minibatch statistics with moving statistics.

2) *Instance Normalization*: In style transfer tasks, Ulyanov *et al.* [30] found that critical improvement could be achieved by replacing batch normalization with instance normalization (IN). Recent image transform tasks [3], [8], [9] confirmed that IN is also useful for improving the qualitative of transform results. Unlike BN that uses the mini-batch statistics, IN only uses the statistics of the instance itself for normalization:

$$\text{IN}(z_r) = \frac{z_r - \mathbb{E}[z_r]}{\sqrt{\text{Var}[z_r]}}. \quad (7)$$

Consequently, the feature statistics IN uses are consistent between the training and inference stages.

3) *Scale and Shift*: A simple normalization operation  $\text{Norm}(\cdot)$  for convolution output may change what it can represent. Therefore, the affine parameters  $\gamma_r$ , and  $\beta_r$  are used for restoring the representation power of the network:

$$\hat{z}_r = \gamma_r \text{Norm}(z_r) + \beta_r. \quad (8)$$

#### IV. POTENTIAL PROBLEMS

From Eq. 4, we know the role of latent code after convolution is to provide a constant offset for the output feature maps. But after the normalization operation, the output distribution indicating the target mapping is destroyed.

##### A. Impaired Consistency of Batch Normalization

For batch normalization, it has the problem that we call mapping inconsistent. Since the network needs to distinguish different mappings based on the mean of feature map, it implies the similar statistical mean is required between different convolutional outputs  $\vec{z}$  of same mapping.

1) *Intra-batch Inconsistency*: Consider this minibatch  $Z^{(1)} = (z^{(1)}, z^{(2)}, z^{(3)})$ , where

$$\begin{aligned} \vec{z}^{(1)} &= (W, V) \times \left( \frac{\vec{x}^{(1)}}{c^{(1)}} \right) = \vec{y}^{(1)} + \vec{o}^{(1)}, \\ \vec{z}^{(2)} &= (W, V) \times \left( \frac{\vec{x}^{(2)}}{c^{(1)}} \right) = \vec{y}^{(2)} + \vec{o}^{(1)}, \\ \vec{z}^{(3)} &= (W, V) \times \left( \frac{\vec{x}^{(3)}}{c^{(1)}} \right) = \vec{y}^{(3)} + \vec{o}^{(1)}. \end{aligned} \quad (9)$$

In batch  $Z^{(1)}$ , different input instances  $\vec{x}^{(1)}, \vec{x}^{(2)}, \vec{x}^{(3)}$  mapping to same domain indicated by latent code  $c^{(1)}$ . But the statistical mean after normalization is inconsistent:

$$\begin{aligned} &\mathbb{E}[\text{BN}(z_r^{(1)})] - \mathbb{E}[\text{BN}(z_r^{(2)})] \\ &= \mathbb{E}[\text{BN}(z_r^{(1)}) - \text{BN}(z_r^{(2)})] \\ &= \mathbb{E}\left[\frac{z_r^{(1)} - z_r^{(2)}}{\sqrt{\text{Var}[Z_r^{(1)}]}}\right] \\ &= \frac{\mathbb{E}[y_r^{(1)} - y_r^{(2)}]}{\sqrt{\text{Var}[Z_r^{(1)}]}}. \end{aligned} \quad (10)$$

It is a very small probability that  $\mathbb{E}[y_r^{(1)} - y_r^{(2)}] = 0$ , which means

$$\mathbb{E}[\text{BN}(z_r^{(1)})] \neq \mathbb{E}[\text{BN}(z_r^{(2)})]. \quad (11)$$

Similarly, we can derive  $\mathbb{E}[\text{BN}(z_r^{(1)})] \neq \mathbb{E}[\text{BN}(z_r^{(2)})] \neq \mathbb{E}[\text{BN}(z_r^{(3)})]$ , as illustrated in Fig. 4(a). Although these three



instances have same mapping, their statistical mean is inconsistent. This property is important for discriminative model since the difference in statistics may represent the different categories. But this distribution inconsistent problem is considered as the shortcoming of BN in style transfer task [31].

2) *Inter-batch Inconsistency*: Besides the inconsistent in single batch, the mapping inconsistent is existed between different batches. Replace  $z^{(3)}$  in  $Z^{(1)}$  with  $z^{(4)}$ , where

$$\vec{z}^{(4)} = (W, V) \times \begin{pmatrix} x^{(3)} \\ c^{(2)} \end{pmatrix} = \vec{y}^{(3)} + \vec{o}^{(2)}. \quad (12)$$

The new batch is  $Z^{(2)} = (\vec{z}^{(1)}, \vec{z}^{(2)}, \vec{z}^{(4)})$ . Here, we use the statistical mean of the same mapping instances to represent the main characteristic of a specific mapping. In batch  $Z^{(1)}$ , the statistical mean of the mappings indicated by  $\vec{c}^{(1)}$  is  $E[\text{BN}(Z^{(1)})] = 0$ , but the mean indicated by  $\vec{c}^{(1)}$  in batch  $Z^{(2)}$  is

$$\begin{aligned} & E[(\text{BN}(z_r^{(1)}), \text{BN}(z_r^{(2)}))] \\ &= \frac{1}{2} E[\text{BN}(z_r^{(1)})] + E[\text{BN}(z_r^{(2)})] \\ &= \frac{E[z_r^{(1)}] + E[z_r^{(2)}] - 2E[Z_r^{(2)}]}{2\sqrt{\text{Var}[Z_r^{(2)}]}} \\ &= \frac{E[Z_r^{(2)}] - E[z_r^{(3)}]}{2\sqrt{\text{Var}[Z_r^{(2)}]}} \\ &= -\frac{1}{2} E[\text{BN}(z_r^{(3)})]. \end{aligned} \quad (13)$$

In most case,  $E[\text{BN}(z_r^{(3)})] \neq 0$ . We learn that the mean of same mapping is always inconsistent in different batches, which means the instance distribution is also inconsistent in the training stage, as shown in Fig. 4(a,b). To address this, the uniform sampling of different mappings is required for each training minibatch, which is difficult when there are a lot of mappings.

Since the mapping inconsistency of BN, the network has to continuously adapt to a new distribution to distinguish different mapping in training stage. Therefore, the network will always experience covariate shift [29] and reduces the performance.

### B. Impaired Diversity of Instance Normalization

The mapping inconsistency of BN is caused by normalizing the feature statistics of a minibatch, so instance normalization does not have this problem since it normalizes the feature statistics of an instance. But IN brings another problem called diversity elimination, like Fig. 4(c).

Consider these two instances  $\vec{z}^{(3)}$  and  $\vec{z}^{(4)}$ . With the same input  $x^{(3)}$ , different mappings are indicated by  $\vec{c}^{(1)}$  and  $\vec{c}^{(2)}$ . Since the latent code convolution output  $\vec{o}_r$  is the constant

channel, the diversity indicated by latent code will be eliminated after IN

$$\begin{aligned} & \text{IN}(z_r^{(3)}) - \text{IN}(z_r^{(4)}) \\ &= \frac{y_r^{(3)} + o_r^{(1)} - E[y_r^{(3)} + o_r^{(1)}]}{\sqrt{\text{Var}[y_r^{(3)} + o_r^{(1)}]}} - \frac{y_r^{(3)} + o_r^{(2)} - E[y_r^{(3)} + o_r^{(2)}]}{\sqrt{\text{Var}[y_r^{(3)} + o_r^{(2)}]}} \\ &= \frac{y_r^{(3)} - E[y_r^{(3)}]}{\sqrt{\text{Var}[y_r^{(3)}]}} - \frac{y_r^{(3)} - E[y_r^{(3)}]}{\sqrt{\text{Var}[y_r^{(3)}]}} = 0, \\ &\Rightarrow \text{IN}(z_r^{(3)}) = \text{IN}(z_r^{(4)}). \end{aligned} \quad (14)$$

### C. Consistency Within Diversity Criteria

With these potential problems, common LCI model is hard to learn the effective mapping indicated by latent code. Motivated, we argue that the feature statistics, especially the mean, represent the target mapping. Therefore, we propose two design criteria to help model multi-mapping. The basic goal is to reduce mapping inconsistency while maintaining diversity. We define the multi-mapping result as  $\phi(\vec{x}, \mathbf{c})$ , where  $\mathbf{c}$  is the original latent code.

1) *Consistency criterion*: To reduce mapping inconsistency, different  $\vec{x}^{(1)}$  and  $\vec{x}^{(2)}$  should produce consistent outputs when given same latent code  $\mathbf{c}$ .

$$E[\phi(\vec{x}^{(1)}, \mathbf{c})] = E[\phi(\vec{x}^{(2)}, \mathbf{c})]. \quad (15)$$

It means that the statistical mean of the mapping function  $\phi(\vec{x}, \mathbf{c})$  should not related to the input  $\vec{x}$ .

2) *Diversity criterion*: To maintain diversity, same input  $\vec{x}$  should produce diversity outputs when given different  $\mathbf{c}^{(1)}$  and  $\mathbf{c}^{(2)}$ . Therefore, the distribution mean of the outputs should not be identical:

$$E[\phi(\vec{x}, \mathbf{c}^{(1)})] \neq E[\phi(\vec{x}, \mathbf{c}^{(2)})]. \quad (16)$$

In other words, the statistical mean of the mapping function  $\phi(\vec{x}, \mathbf{c})$  should related to the input  $\mathbf{c}$ .

## V. CENTRAL BIASING NORMALIZATION

### A. Formulation

Here, we propose center biasing operation for common normalization to meets the design criteria and maintains the stable distribution after normalization. Specifically, we first eliminate the offset of feature maps to meet the consistency criterion and then append a bias to follow the diversity criterion. The central biasing normalization (CBN) can be represent as

$$\text{CBN}(y_r, \mathbf{c}) = \text{Norm}(y_r) - E[\text{Norm}(y_r)] + b_r(\mathbf{c}), \quad (17)$$

where

$$b_r(\mathbf{c}) := \tanh(f(\mathbf{c})). \quad (18)$$

As shown in Eq.17,  $\text{Norm}(\cdot)$  represents the common normalization.  $b_r(\mathbf{c})$  is the bias for  $r$ -th output feature map, which is initialized simply by applying an affine transformation  $f$

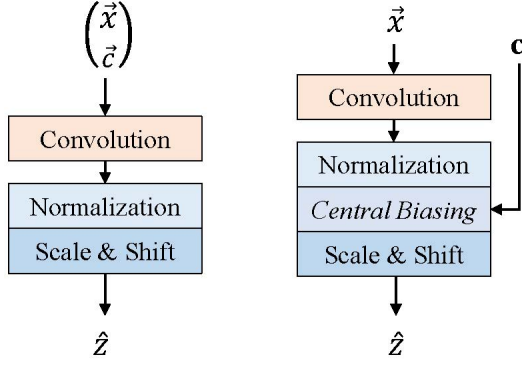


Fig. 5. Left: a traditional convolutional block with latent code injection. Right: a convolutional block with proposed center biasing normalization.

to the latent code. Use this initialized bias  $f(\mathbf{c})$  also meet the design criteria, but we argue that violates the original intention of normalization. To accelerate deep network training, the normalization operation is applied to reduce internal covariate shift of network by ensuring the input distribution is stable for nonlinear layer. But without any constraint, the feature distribution after adding bias  $f(\mathbf{c})$  is unknown since there is no constraint on the range of bias. To stable the output distribution, we append a  $\tanh$  function to constrain range of bias. The final bias for feature map is defined as Eq. 18.

The mean of feature is  $E[\text{CBN}(y_r, \mathbf{c})] = b_r(\mathbf{c})$ , where  $b_r(\mathbf{c}) \in [-1, 1]$ . With the scale and shift operation, the distribution after normalization is stable for the next layer.

### B. Proof

Without the central biasing, batch normalization does not meet the consistency criterion.

$$\begin{aligned}
 E[\text{BN}(z_r)] &= E\left[\frac{z_r - E[Z_r]}{\sqrt{\text{Var}[Z_r]}}\right] = \frac{E[z_r] - E[Z_r]}{\sqrt{\text{Var}[Z_r]}} \\
 &= \frac{E[y_r + o_r] - E[Y_r + O_r]}{\sqrt{\text{Var}[Z_r]}} \\
 &= \frac{E[y_r + o_r] - E[Y_r + O_r]}{\sqrt{\text{Var}[Z_r]}} \\
 &= \frac{E[y_r - E[Y_r]]}{\sqrt{\text{Var}[Z_r]}} + \frac{E[o_r - E[O_r]]}{\sqrt{\text{Var}[Z_r]}}. \quad (19)
 \end{aligned}$$

From Eq. 19, we learn that the mean value after BN relates to the input  $\vec{x}$  and minibatch.

As for instance normalization, it violates the diversity criterion.

$$E[\text{IN}(z_r)] = E\left[\frac{z_r - E[z_r]}{\sqrt{\text{Var}[z_r]}}\right] = \frac{E[z_r] - E[z_r]}{\sqrt{\text{Var}[z_r]}} = 0. \quad (20)$$

After applying central biasing, these normalization operations will meet the design criteria.

$$\begin{aligned}
 E[\text{CBN}(y_r, \mathbf{c})] &= E[\text{Norm}(y_r) - E[\text{Norm}(y_r)] + b_r(\mathbf{c})] \\
 &= E[\text{Norm}(y_r)] - E[E[\text{Norm}(y_r)]] + E[b_r(\mathbf{c})] \\
 &= E[b_r(\mathbf{c})]. \quad (21)
 \end{aligned}$$

TABLE I  
THE NETWORK ARCHITECTURE OF CBG. “ $C \times K \times L \text{ Conv } S_n P_m$ ” DENOTES  $C$   $n$ -STRIDE CONVOLUTIONAL FILTERS WITH  $K \times L$  KERNEL SIZE AND  $m$  SIZED ZERO-PADDING OR REFLECTION-PADDING.  $H$  AND  $W$  ARE THE HEIGHT AND WIDTH OF THE INPUT IMAGE, RESPECTIVELY.

Convolution	Norm	Activation	Output Size
$64 \times 7 \times 7 \text{ Conv } S1 P3$	CBN	ReLU	$64 \times H \times W$
$128 \times 4 \times 4 \text{ Conv } S2 P1$	CBN	ReLU	$128 \times \frac{H}{2} \times \frac{W}{2}$
$256 \times 4 \times 4 \text{ Conv } S2 P1$	CBN	ReLU	$256 \times \frac{H}{4} \times \frac{W}{4}$
$256 \times 3 \times 3 \text{ Res } S1 P1$	CBN	ReLU	$256 \times \frac{H}{4} \times \frac{W}{4}$
$256 \times 3 \times 3 \text{ Res } S1 P1$	CBN	ReLU	$256 \times \frac{H}{4} \times \frac{W}{4}$
$256 \times 3 \times 3 \text{ Res } S1 P1$	CBN	ReLU	$256 \times \frac{H}{4} \times \frac{W}{4}$
$256 \times 3 \times 3 \text{ Res } S1 P1$	CBN	ReLU	$256 \times \frac{H}{4} \times \frac{W}{4}$
$256 \times 3 \times 3 \text{ Res } S1 P1$	CBN	ReLU	$256 \times \frac{H}{4} \times \frac{W}{4}$
$128 \times 4 \times 4 \text{ TrConv } S2 P1$	BN/IN	ReLU	$128 \times \frac{H}{2} \times \frac{W}{2}$
$64 \times 4 \times 4 \text{ TrConv } S2 P1$	BN/IN	ReLU	$64 \times H \times W$
$3 \times 7 \times 7 \text{ TrConv } S1 P3$	/	Tanh	$3 \times H \times W$

For specific normalizations BN and IN, CBN can be simplified as CBBN and CBIN respectively:

$$\text{CBBN}(y_r, \mathbf{c}) = \frac{y_r - E[y_r]}{\sqrt{\text{Var}[\mathbf{Y}_r]}} + b_r(\mathbf{c}), \quad (22)$$

$$\text{CBIN}(y_r, \mathbf{c}) = \frac{y_r - E[y_r]}{\sqrt{\text{Var}[y_r]}} + b_r(\mathbf{c}). \quad (23)$$

It should be noted that CBBN eliminates the instance mean  $E[y_r]$  instead of batch mean  $E[\mathbf{Y}_r]$  and the output variance of distribution depend on the batch instead of instance like CBIN.

## VI. EXPERIMENTS

As mentioned in above sections, the multi-mapping tasks can be classified to multi-modal tasks and multi-domain tasks. We choose the state-of-the-art models of each task as our baselines. Specifically, we adopt BicycleGAN [9] for multi-modal tasks and StarGAN [8] for multi-domain transform tasks.

### A. Network Architecture

Instead of spatial replicating and concatenating into the inputs, we inject the latent code into the normalization layers by replacing traditional normalization with central biasing normalization, as shown in Fig. 5. We adapt the common encoder-decoder architecture [3], [8], [32] to build the generator, which contains two stride-2 convolution layers for downsampling, six residual blocks [33] and two stride-2 transposed convolution layers for upsampling. The normalization layers in the downsampling and residual blocks are replaced with central biasing normalization layers to build a multi-mapping generator, which we refer to as central biasing generator (CBG). The network architecture is shown in Table I.

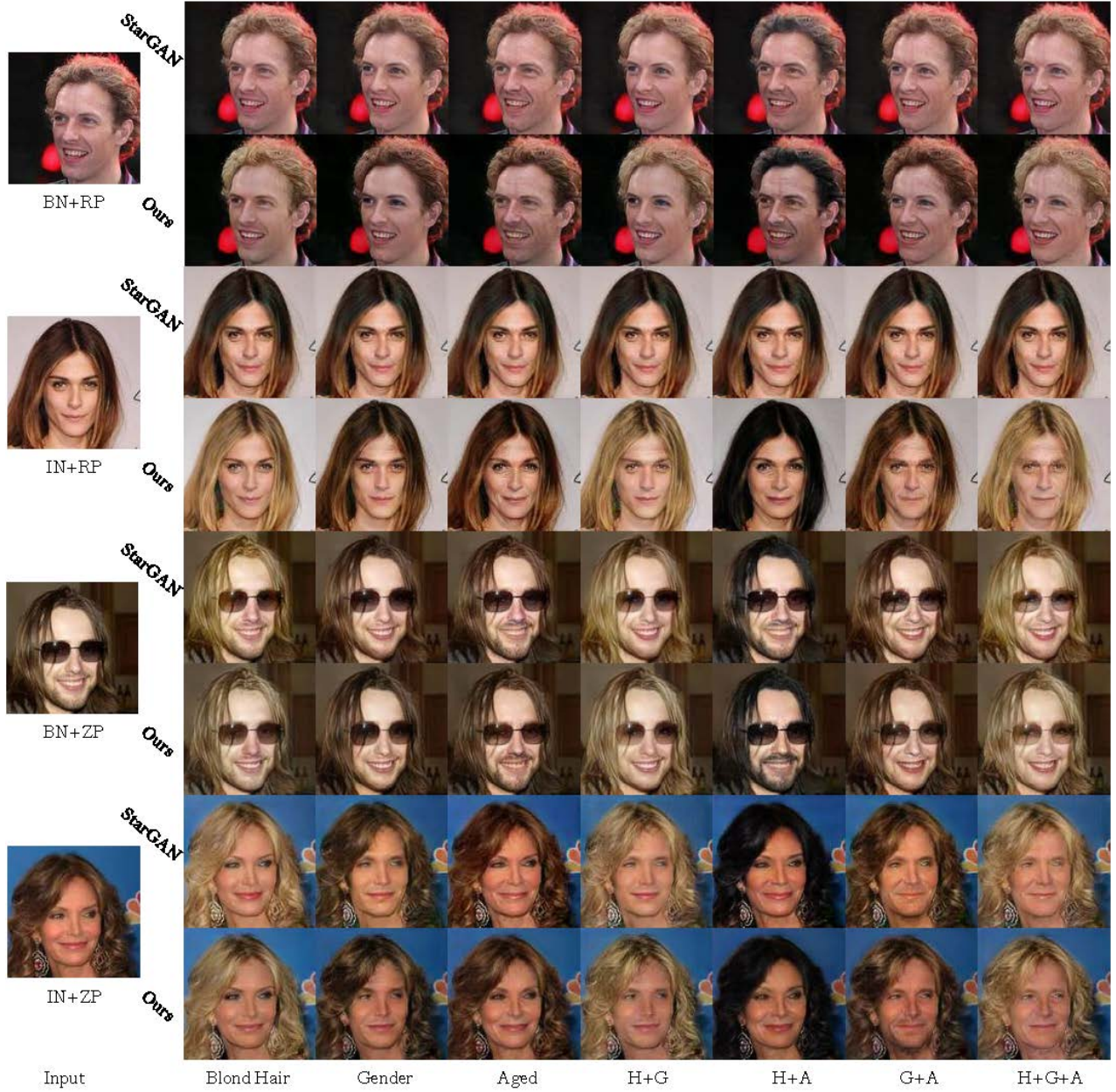


Fig. 6. Facial attribute transfer results. The first column shows the input image, next three columns show the single attribute transform results, and the rest of columns show the multi-attribute transfer results. H: Hair color, G: Gender, A: Aged.

TABLE II  
THE CLASSIFICATION ACCURACY FOR FACIAL ATTRIBUTE TRANSFER RESULTS.

Method	Hair color	Gender	Aged	Average
BN+RP StarGAN	70.90	61.16	61.57	64.54
Ours	<b>81.93</b>	<b>68.00</b>	<b>63.21</b>	<b>71.05</b>
IN+RP StarGAN	33.33	50.00	50.00	44.44
Ours	<b>96.46</b>	<b>88.55</b>	<b>86.05</b>	<b>90.36</b>
BN+ZP StarGAN	84.25	<b>79.53</b>	66.09	76.62
Ours	<b>88.63</b>	76.32	<b>67.76</b>	<b>77.57</b>
IN+ZP StarGAN	95.25	88.38	86.05	89.89
Ours	<b>95.74</b>	<b>90.20</b>	<b>86.11</b>	<b>90.68</b>
Real images	91.56	97.25	88.74	92.52

TABLE III  
THE PERCEPTUAL DISTANCE FOR EDGES2PHOTOS AND LABEL2PHOTOS TASKS.

Method	edge→photo	label→photo	Average
BN+RP BicycleGAN	0.069	0.629	0.349
Ours	<b>0.867</b>	<b>1.499</b>	<b>1.183</b>
IN+RP BicycleGAN	1.025	1.027	1.026
Ours	<b>1.652</b>	<b>1.417</b>	<b>1.535</b>
BN+ZP BicycleGAN	0.492	1.281	0.887
Ours	<b>0.754</b>	<b>1.641</b>	<b>1.198</b>
IN+ZP BicycleGAN	1.106	1.318	1.212
Ours	<b>1.637</b>	<b>1.562</b>	<b>1.599</b>
Real images	3.481	3.233	3.357





Fig. 7. Edges2Photos results. The first column shows the input image and the remaining columns are the results transfer from sample latent code.

### B. Multi-domain Translation

1) *Dataset*: Facial attribute transfer is a typical multi-domain translation problem. We randomly select 2,000 images from 202,599 face images in CelebA dataset [34] of celebrities as test set and remain the rest of images for training set. Then we crop the images to  $178 \times 178$ , and resize them to  $128 \times 128$ . Seven facial attributes are selected to training the multi-domain transform models: hair color (black, blond, brown), gender (male/female), and age (young/old).

2) *Baseline*: To model multi-domain mappings with a single model, StarGAN introduces the auxiliary classifier [23] for the discriminator. Since StarGAN use the attribute label as the latent code  $\mathbf{c}$ , the latent space is discrete and the state of  $\mathbf{c}$  is limited.

3) *Metric*: To judge the specific domains image translation capabilities, we compare the classification accuracy of facial attributes on synthesized images. We use the ResNet-18 [33] which is pre-trained on the ImageNet dataset [35], and fine-tuned it for multi-label classification on the CelebA dataset (10-fold cross validation in training set). We use the same training set for each image translation models and translate all possible combinations (12 domain of facial attributes) from the unseen test images.

### C. Multi-modal Translation

1) *Datasets*: We perform the evaluate on several multi-model translation tasks, including Edges2Photos [36], [37], labels2Photos [38], night2day [39]. We resize all of the images to  $128 \times 128$ .



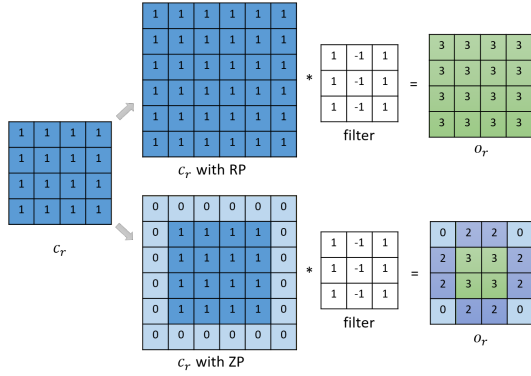


Fig. 8. Different padding operations. The first column is the source latent code channel  $c_r$ . The first row in the rest columns is the convolution with reflection-padding, next row is the the convolution with zero-padding.

2) *Baseline*: To model a distribution of possible outputs in a conditional generative modeling setting, BicycleGAN combines the VAE-GAN [24] and LR-GAN [12], [25], [26] objectives for encouraging a bijective mapping between the latent and output spaces. Since BicycleGAN use the encoder with a Gaussian assumption to extract the latent code  $c$ , the latent space is continuous and the state of  $c$  is varied.

3) *Metric*: We compare the diversity of different models by computing averaged perceptual distance in feature space. As suggested in [9], we use the cosine similarity (CosSim) to evaluate the distance in the feature space of VGG-16 network [40] pre-trained in ImageNet. We average across spatial dimensions and sum across the five convolution layers preceding the pool layers. As in Zhu *et al.* [9], the perceptual distance is defined as  $(5.0 - \sum_{i=1}^5 \text{CosSim}_i)$ . The larger the perceptual distance, the greater the difference between two images. To evaluate the diversity of different models, we randomly sample an input image and use a pair of random latent code to generate images. Then we compute the average distance between 2,000 pairs of generated images.

#### D. Verification of Potential Problems

As discussed in Sec. IV, existing latent code injection model has some potential problems when modeling multi-mapping. But in the existing works [8], [9], why do similar convolution pipeline with instance normalization can still work? The reason is that these networks introduce zero-padding (ZP) before the convolution operation, which aims to control the spatial size of the output volume. After zero-padding, the latent code channel of the input volume is no longer a constant plane but has a circle of zero boundaries. Through convolutional operation, the latent code convolution output  $\vec{o}_r$  in Eq. 4 is not the constant channel. The convolution activation boundaries give the possible of the feature maps to keep diversity in non-boundary areas after instance normalization. However, such problems still exist if we unequip the zero-padding or use other padding strategy, such as reflection-padding (RP). To validate the problems, we replace ZP with RP in StarGAN and BicycleGAN during the following experiments.

1) *Impaired Consistency of BN*: To verify the mapping inconsistency of batch normalization, we replace the original

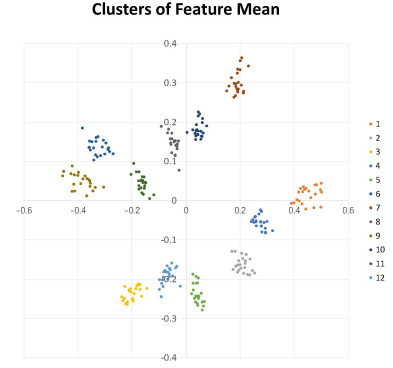


Fig. 9. The k-means cluster results from 2 dimensional statistical data. Different colors represent different mappings indicated by latent code.

generator with the proposed CBG model under the settings of CBBN. The qualitative comparison results are shown in Fig. 6, 7. To quantitative analysis the model performance, we test the diversity and classification error of these models, as shown in Table II, III. We got the quantitative results that comply with qualitative performance. Both the latent code injection models produce realistic outputs but lose output diversity. Conversely, CBG presents various outputs while maintaining realistic. The main difference between LCI models and CBG is the mean of feature maps after normalization. The mapping inconsistency of BN seriously affects the performance of the network. During training time, the network can hardly learn the effective mapping since the feature mean of same mapping is always changing. After correcting the inconsistency, CBG effectively learn the mapping indicated by the latent code.

2) *Impaired Diversity of IN*: In order to explore the mapping elimination of instance normalization, we equip the instance normalization in BicycleGAN and StarGAN. Meanwhile, we use CBG as a comparison under the CBIN settings. We employ the original implementation of BicycleGAN with the UNet generator [41] which does not equip normalization in the first convolution layer. Since the effect of latent code is eliminated after IN, StarGAN fails to perform domain translation as shown in Fig. 6. Without normalization of the first convolution, BicycleGAN can retain the diversity indicated by latent code, as shown in Fig. 7. But the visual quality is not very satisfactory. It suggests that discarding normalization is not a good idea to retain diversity in the deep network. Under the similar settings, CBG shows more satisfactory results.

#### E. Discussion

1) *Role of Padding*: To study the role of padding strategy for multi-mapping model, we compared the performance of models under different padding settings. As the qualitative results in Fig. 6, 7, we can observe that ZP mode is better than RP mode for traditional LCI. The observation is also faithfully shown on quantitative analysis. Let us revisit the padding strategy shown in Fig. 8. As discussed in the previous sections, latent code just provides a constant offset in RP mode. So the mapping inconsistency and mapping elimination problems still



Fig. 10. label2photos results with different length of latent code.

exist. For ZP mode, the convolution of latent code provides the feature map that contains non-constant boundaries and constant center region. Therefore, the network has the ability to control the distribution of feature for different mappings after normalization. Since the feature mean is normalized to zero after IN, the LCI model with ZP against our diversity criteria on the surface. But apart from the non-constant boundaries, the feature map of latent code is also to provide a constant offset. We think the key to distinguish different mappings is also the mean in non-boundary feature region.

After testing the StarGAN under the settings of IN+ZP, we found the feature mean and target mapping are strongly related. We first sample the feature maps  $\vec{z}$  which are the normalization output with latent code injection convolution operation. In the test images with 12 conversions, the feature mean is calculated without considering boundary area affected by padding operation. We use principal component analysis (PCA) to reduce the dimension of the statistical mean channels (64 to 6). After performing k-means ( $k=12$ ) clustering in the low dimensional data, we found that each cluster represents a kind of mapping. We reduce the data dimension to 2 using PCA for visualization, as shown in Fig. 9. This phenomenon implies zero padding of LCI model help the model to perform multi-mapping by control the distribution of feature. The role of ZP in traditional LCI is similar to central biasing normalization. Since there is no need to optimize redundant parameters of  $V$  in Eq. 3, CBG is more straightforward and effective to control the mappings and get better results.

2) *CBBN and CBIN*: In our design criteria, we assume the crucial statistics of multi-mapping model is the mean of feature maps. There is no constraint on the other statistical property, such as variance. Actually, the difference between of CBBN and CBIN is the feature variance of same mapping. After CBBN, the statistical variance of feature in the same mapping is not identical since it uses the variance of the batch. After CBIN, the statistical variance of feature is normalized to 1 since it uses the variance of instance. According to the results in above sections, we can learn that CBIN always outperform CBBN. It means a stable data distribution is essential for the network to learn the mapping.

3) *Effects of Latent Code Length*: As in Zhu *et al.* [9], we explore the effect of latent code length on model performance. Under varying number of dimensions of latent

TABLE IV  
GENERATOR PARAMETERS WITH DIFFERENT LENGTH OF LATENT CODE.

Base model	BicycleGAN	BNG
	39.9M	8M
$ z  = 2$	+78K	<b>+6.9K</b>
$ z  = 8$	+312K	<b>+27.5K</b>
$ z  = 128$	+4.9M	<b>+440K</b>
$ z  = 256$	+9.75M	<b>+880K</b>

codes  $\{2, 8, 128, 256\}$ , we test the default BicycleGAN, which uses IN and ZP, and CBG with similar settings. Similar the results of Zhu *et al.* [9], a high-dimensional latent code can potentially encode more information for image generation at the cost of making sampling quite difficult. CBG shows stable performance when the dimension of latent code is enough, as shown in Fig. 10. In addition, CBG is low cost for increasing the dimension of latent code. Table IV shows the generator parameter number compared with BicycleGAN and CBG. Due to replication of latent code in LCI model, the convolutional parameters for latent code (convolution matrix  $V$  in Eq. 3) are redundant. For a fair comparison, we just use the suggested latent code dimension 8 [9] in other experiments.

TABLE V  
THE AVERAGE RECONSTRUCTION LOSS FOR EDGES2PHOTOS AND LABEL2PHOTOS TASKS.

Method		edge→photo	label→photo	Average
BN+RP	BicycleGAN	0.094	0.152	0.123
	Ours	<b>0.049</b>	<b>0.142</b>	<b>0.096</b>
IN+RP	BicycleGAN	0.051	0.148	0.100
	Ours	<b>0.034</b>	<b>0.132</b>	<b>0.083</b>
BN+ZP	BicycleGAN	0.061	0.138	0.100
	Ours	<b>0.049</b>	<b>0.136</b>	<b>0.093</b>
IN+ZP	BicycleGAN	0.048	<b>0.133</b>	0.091
	Ours	<b>0.034</b>	<b>0.133</b>	<b>0.084</b>

4) *Translation Consistency*: Besides the diversity of different mappings, the consistency of same mappings should be considered for multi-mapping model. For multi-domain translation task, it can use the domain classification accuracy to as metric, as shown in Table II. For multi-modal translation task, we use the latent code encoded by ground truth to indicated the image generation, and calculate the reconstruction loss to measure the consistency of model. Table V shows that CBG



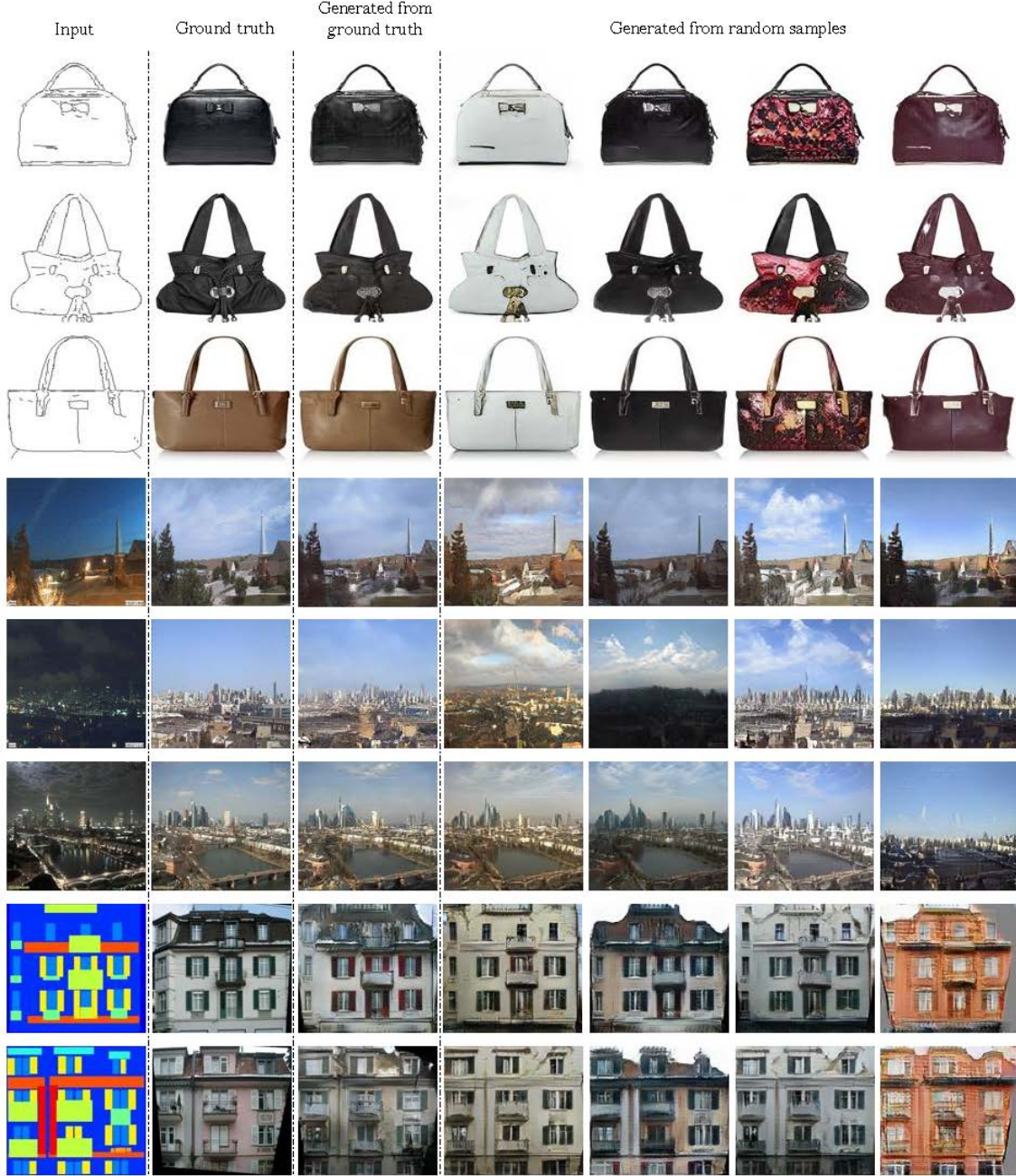


Fig. 11. Diversity and consistency results of multi-modal translation. The left column is the input images. The second shows the ground truth output. The third shows the generated outputs with latent code encoded from ground truth. The rest columns show the generated outputs using different random latent code. The latent code is fixed in each column. Therefore, results from the same column show the consistency of our network while results from different columns show the diversity of our network.

consistency is better than LCI model in most case. More CBG consistency results are shown in Fig. 11.

## VII. CONCLUSIONS

In this paper, we revisit the latent code injection in multi-mapping convolution neural network to show the role of latent code. By derivation, we find common normalization is not suitable for multi-mapping tasks. Therefore, we present the

diversity and consistency criterion as guides to designing the multi-mapping model. Specifically, we propose the central biasing normalization to replace LCI for meeting the design criteria. We apply our method to multi-domain and multi-modal tasks and show it is effectively in different tasks.



## REFERENCES

- [1] P. Isola, J.-Y. Zhu, T. Zhou, and A. A. Efros, “Image-to-image translation with conditional adversarial networks,” in *Computer Vision and Pattern Recognition (CVPR), 2017 IEEE Conference on*, 2017.
- [2] R. Zhang, P. Isola, and A. A. Efros, “Colorful image colorization,” *European Conference on Computer Vision*, 2016.
- [3] J.-Y. Zhu, T. Park, P. Isola, and A. A. Efros, “Unpaired image-to-image translation using cycle-consistent adversarial networks,” in *Computer Vision (ICCV), 2017 IEEE International Conference on*, 2017.
- [4] Z. Yi, H. Zhang, P. Tan, and M. Gong, “Dualgan: Unsupervised dual learning for image-to-image translation,” in *IEEE International Conference on Computer Vision*, 2017, pp. 2868–2876.
- [5] T. Kim, M. Cha, H. Kim, J. K. Lee, and J. Kim, “Learning to discover cross-domain relations with generative adversarial networks,” in *International Conference on Machine Learning*, 2017, pp. 1857–1865.
- [6] M.-Y. Liu, T. Breuel, and J. Kautz, “Unsupervised image-to-image translation networks,” in *Advances in Neural Information Processing Systems*, 2017, pp. 700–708.
- [7] G. Lample, N. Zeghidour, N. Usunier, A. Bordes, L. Denoyer *et al.*, “Fader networks: Manipulating images by sliding attributes,” in *Advances in Neural Information Processing Systems*, 2017, pp. 5969–5978.
- [8] Y. Choi, M. Choi, M. Kim, J.-W. Ha, S. Kim, and J. Choo, “Stargan: Unified generative adversarial networks for multi-domain image-to-image translation,” *arXiv preprint arXiv:1711.09020*, 2017.
- [9] J.-Y. Zhu, R. Zhang, D. Pathak, T. Darrell, A. A. Efros, O. Wang, and E. Shechtman, “Toward multimodal image-to-image translation,” in *Advances in Neural Information Processing Systems 30*, 2017.
- [10] I. Goodfellow, J. Pouget-Abadie, M. Mirza, B. Xu, D. Warde-Farley, S. Ozair, A. Courville, and Y. Bengio, “Generative adversarial nets,” in *Advances in neural information processing systems*, 2014, pp. 2672–2680.
- [11] X. Mao, Q. Li, H. Xie, R. Y. Lau, Z. Wang, and S. P. Smolley, “Least squares generative adversarial networks,” in *2017 IEEE International Conference on Computer Vision (ICCV)*. IEEE, 2017, pp. 2813–2821.
- [12] X. Chen, Y. Duan, R. Houthoofd, J. Schulman, I. Sutskever, and P. Abbeel, “Infogan: Interpretable representation learning by information maximizing generative adversarial nets,” in *Advances in Neural Information Processing Systems*, 2016, pp. 2172–2180.
- [13] M. Arjovsky, S. Chintala, and L. Bottou, “Wasserstein generative adversarial networks,” in *International Conference on Machine Learning*, 2017, pp. 214–223.
- [14] I. Gulrajani, F. Ahmed, M. Arjovsky, V. Dumoulin, and A. C. Courville, “Improved training of wasserstein gans,” in *Advances in Neural Information Processing Systems*, 2017, pp. 5769–5779.
- [15] A. Radford, L. Metz, and S. Chintala, “Unsupervised representation learning with deep convolutional generative adversarial networks,” *ICLR*, 2016.
- [16] D. Pathak, P. Krahenbuhl, J. Donahue, T. Darrell, and A. A. Efros, “Context encoders: Feature learning by inpainting,” in *Proceedings of the IEEE Conference on Computer Vision and Pattern Recognition*, 2016, pp. 2536–2544.
- [17] C. Ledig, L. Theis, F. Huszar, J. Caballero, A. Cunningham, A. Acosta, A. Aitken, A. Tejani, J. Totz, Z. Wang *et al.*, “Photo-realistic single image super-resolution using a generative adversarial network,” in *Computer Vision and Pattern Recognition (CVPR), 2017 IEEE Conference on*, 2017.
- [18] S. Reed, Z. Akata, X. Yan, L. Logeswaran, B. Schiele, and H. Lee, “Generative adversarial text to image synthesis,” in *International Conference on Machine Learning*, 2016, pp. 1060–1069.
- [19] A. Brock, T. Lim, J. M. Ritchie, and N. Weston, “Neural photo editing with introspective adversarial networks,” *ICLR*, 2017.
- [20] M. Mirza and S. Osindero, “Conditional generative adversarial nets,” *arXiv preprint arXiv:1411.1784*, 2014.
- [21] D. P. Kingma and M. Welling, “Auto-encoding variational bayes,” *ICLR*, 2014.
- [22] M.-Y. Liu and O. Tuzel, “Coupled generative adversarial networks,” in *Advances in neural information processing systems*, 2016, pp. 469–477.
- [23] A. Odena, C. Olah, and J. Shlens, “Conditional image synthesis with auxiliary classifier gans,” *arXiv preprint arXiv:1610.09585*, 2016.
- [24] A. B. L. Larsen, S. K. Sønderby, H. Larochelle, and O. Winther, “Autoencoding beyond pixels using a learned similarity metric,” in *33rd International Conference on Machine Learning*, 2016.
- [25] J. Donahue, P. Krähenbühl, and T. Darrell, “Adversarial feature learning,” *ICLR*, 2016.
- [26] V. Dumoulin, I. Belghazi, B. Poole, O. Mastropietro, A. Lamb, M. Arjovsky, and A. Courville, “Adversarially learned inference,” *ICLR*, 2016.
- [27] J. Cong and B. Xiao, “Minimizing computation in convolutional neural networks,” in *International conference on artificial neural networks*. Springer, 2014, pp. 281–290.
- [28] S. Ioffe and C. Szegedy, “Batch normalization: Accelerating deep network training by reducing internal covariate shift,” in *International conference on machine learning*, 2015, pp. 448–456.
- [29] H. Shimodaira, “Improving predictive inference under covariate shift by weighting the log-likelihood function,” *Journal of statistical planning and inference*, vol. 90, no. 2, pp. 227–244, 2000.
- [30] D. Ulyanov, A. Vedaldi, and V. Lempitsky, “Instance normalization: The missing ingredient for fast stylization,” *arXiv preprint arXiv:1607.08022*, 2016.
- [31] X. Huang and S. Belongie, “Arbitrary style transfer in real-time with adaptive instance normalization,” in *ICCV*, 2017.
- [32] J. Johnson, A. Alahi, and L. Fei-Fei, “Perceptual losses for real-time style transfer and super-resolution,” in *European Conference on Computer Vision*. Springer, 2016, pp. 694–711.
- [33] K. He, X. Zhang, S. Ren, and J. Sun, “Deep residual learning for image recognition,” in *Proceedings of the IEEE conference on computer vision and pattern recognition*, 2016, pp. 770–778.
- [34] Z. Liu, P. Luo, X. Wang, and X. Tang, “Deep learning face attributes in the wild,” in *Proceedings of the IEEE International Conference on Computer Vision*, 2015, pp. 3730–3738.
- [35] O. Russakovsky, J. Deng, H. Su, J. Krause, S. Satheesh, S. Ma, Z. Huang, A. Karpathy, A. Khosla, M. Bernstein *et al.*, “Imagenet large scale visual recognition challenge,” *International Journal of Computer Vision*, vol. 115, no. 3, pp. 211–252, 2015.
- [36] A. Yu and K. Grauman, “Fine-grained visual comparisons with local learning,” in *Proceedings of the IEEE Conference on Computer Vision and Pattern Recognition*, 2014, pp. 192–199.
- [37] J.-Y. Zhu, P. Krähenbühl, E. Shechtman, and A. A. Efros, “Generative visual manipulation on the natural image manifold,” in *European Conference on Computer Vision*. Springer, 2016, pp. 597–613.
- [38] R. Tyleček and R. Šára, “Spatial pattern templates for recognition of objects with regular structure,” in *German Conference on Pattern Recognition*. Springer, 2013, pp. 364–374.
- [39] P.-Y. Laffont, Z. Ren, X. Tao, C. Qian, and J. Hays, “Transient attributes for high-level understanding and editing of outdoor scenes,” *ACM Transactions on Graphics (proceedings of SIGGRAPH)*, vol. 33, no. 4, 2014.
- [40] K. Simonyan and A. Zisserman, “Very deep convolutional networks for large-scale image recognition,” *Computer Science*, 2014.
- [41] O. Ronneberger, P. Fischer, and T. Brox, “U-net: Convolutional networks for biomedical image segmentation,” in *International Conference on Medical image computing and computer-assisted intervention*. Springer, 2015, pp. 234–241.